Highly branched isoprenoids for Southern Ocean semi-quantitative sea ice reconstructions: a pilot study from the Western Antarctic Peninsula

Maria-Elena Vorrath[1], Juliane Müller[1,2,3], Oliver Esper[1], Gesine Mollenhauer[1,2], Christian Haas[1], Enno Schefuß[2], Kirsten Fahl[1]

[1]Alfred Wegener Institute, Helmholtz Centre for Polar and Marine Research, Bremerhaven, Germany

[2]MARUM – Center for Marine Environmental Sciences, University of Bremen, Germany

[3]Department of Geosciences, University of Bremen, Germany

Correspondence to: Maria-Elena Vorrath, maria-elena.vorrath@awi.de

Abstract. Organic geochemical and micropaleontological analyses of surface sediments collected in the southern Drake Passage and the Bransfield Strait, Antarctic Peninsula, enable a proxy-based reconstruction of recent sea ice conditions in this climate sensitive area. The distribution of the sea ice biomarker $IPSO_{25}$ supports earlier suggestions that the source diatoms seem to be common in near-coastal environments characterized by an annually recurring sea ice cover. We here propose and evaluate the combination of $IPSO_{25}$ with a more unsaturated highly branched isoprenoid alkene and phytosterols and introduce the $PIPSO_{25}$ index as a potentially semi-quantitative sea ice proxy. This organic geochemical approach is complemented with diatom data. $PIPSO_{25}$ sea ice estimates are used to discriminate between areas characterized by permanently ice-free conditions, seasonal sea ice cover and extended sea ice cover. These trends are consistent with satellite sea ice data and winter sea ice concentrations estimated by diatom transfer functions. Minor offsets between proxy-based and satellite-based sea ice data are attributed to the different time intervals recorded within the sediments and the instrumental records from the study area, which experienced rapid environmental changes during the past 100 years.

Key Words: biomarker, $IPSO_{25}$, sea ice, Bransfield Strait, satellite observation

1 Introduction

In the last century, the Western Antarctic Peninsula (WAP) has undergone a rapid warming of the atmosphere of 3.7 ± 1° C, which exceeds several times the average global warming (Vaughan et al., 2003). Simultaneously, a

reduction in sea ice coverage (Parkinson and Cavalieri, 2012), a shortening of the sea ice season (Parkinson, 2002) and a decreasing sea ice extent of ~4-10 % per decade (Liu et al., 2004) are recorded in the adjacent Bellingshausen Sea. The loss of seasonal sea ice and increased melt water fluxes impact the formation of deep and intermediate waters, the ocean-atmosphere-exchange of gases and heat, the primary production and higher trophic levels (Arrigo et al., 1997; Morrison et al., 2015; Orsi et al., 2002; Rintoul, 2007). Since the start of satellite-based sea ice observations, however, a slight increase in total Antarctic sea ice extent has been documented, which contrasts the significant decrease of sea ice in Western Antarctica, especially around the WAP (Hobbs et al., 2016).

For an improved understanding of the oceanic and atmospheric feedback mechanisms associated with the observed changes in sea ice coverage, reconstructions of past sea ice conditions in climate sensitive areas such as the WAP are of increasing importance. A common approach for sea ice reconstructions in the Southern Ocean is based on the investigation of sea ice associated diatom assemblages preserved in marine sediments (Bárcena et al., 1998; Gersonde and Zielinski, 2000; Heroy et al., 2008; Leventer, 1998; Minzoni et al., 2015). By means of transfer functions, this approach can provide quantitative estimates of a paleo sea ice coverage (Crosta et al., 1998; Esper and Gersonde, 2014a). The application of diatoms for paleoenvironmental studies, however, can be limited by the selective dissolution of biogenic opal frustules (Burckle and Cooke, 1983; Esper and Gersonde, 2014b) in the photic zone (Ragueneau et al., 2000) and in surface sediments (Leventer, 1998). As an alternative or additional approach to diatom studies, Massé et al. (2011) proposed the use of a specific biomarker lipid – a diunsaturated highly branched isoprenoid alkene (HBI $C_{25:2}$, Fig. 1) – for Southern Ocean sea ice reconstructions. The HBI diene was first described by Nichols et al. (1988) from sea ice diatoms. ^{13}C isotopic analyses of the HBI diene suggest a sea ice origin for this molecule (Sinninghe Damsté et al., 2007; Massé et al., 2011) and this is further corroborated by the identification of the sea ice diatom *Berkeleya adeliensis* as a producer of this HBI diene (Belt et al., 2016). In a survey of surface sediments collected from proximal sites around Antarctica, Belt et al. (2016) note a widespread sedimentary occurrence of the HBI diene and – by analogy with the Arctic HBI monoene termed IP_{25} (Belt et al., 2007) – proposed the term $IPSO_{25}$ (Ice Proxy for the Southern Ocean with 25 carbon atoms) as a new name for this biomarker.

In previous studies, an HBI triene (HBI $C_{25:3}$; Fig. 1) found in polar and sub-polar phytoplankton samples (Massé et al., 2011) has been considered alongside $IPSO_{25}$ and the ratio of $IPSO_{25}$ to this HBI triene hence has been interpreted as a measure for the relative contribution of organic matter derived from sea ice algae versus open water phytoplankton (Massé et al., 2011; Collins et al., 2013; Etourneau et al., 2013; Barbara et al., 2013, 2016). Collins et al. (2013) further suggested that the HBI triene might reflect phytoplankton productivity in marginal ice zones (MIZ) and, based on the observation of elevated HBI triene concentrations in East Antarctic MIZ surface

waters, this has been strengthened by Smik et al. (2016a). Known source organisms of $C_{25:3}$ HBI trienes (Fig. 1 shows molecular structures of both the E- and Z-isomer) are, for example, *Rhizosolenia* and *Pleurosigma* diatom species (Belt et al., 2000, 2017). In the subpolar North Atlantic, the HBI Z-triene has been used to further modify the so-called PIP_{25} index (Smik et al., 2016b) - an approach for semi-quantitative sea ice estimates. Initially, PIP_{25} was based on the employment of phytoplankton-derived sterols, such as brassicasterol and dinosterol (Kanazawa et al., 1971; Volkman, 2003), to serve as open-water counterparts, while IP_{25} reflects the occurrence of a former sea ice cover (Belt et al., 2007; Müller et al., 2009, 2011). Consideration of these different types of biomarkers helps to discriminate between ice-free and permanently ice-covered ocean conditions, both resulting in a lack of IP_{25} and $IPSO_{25}$, respectively (for further details see Belt, 2018; Belt and Müller, 2013a). Uncertainties in the source-specificity of brassicasterol (Volkman, 1986) and its identification in Arctic sea ice samples (Belt et al., 2013), however, require caution when pairing this sterol with a sea ice biomarker lipid for Arctic sea ice reconstructions. In this context, we note that Belt et al. (2018) reported that brassicasterol is not evident in the $IPSO_{25}$ producing sea ice diatom *Berkeleya adeliensis*. While the applicability of HBIs (and sterols) to reconstruct past sea ice conditions has been thoroughly investigated in the Arctic Ocean (Belt, 2018; Stein et al., 2012; Xiao et al., 2015), only two studies document the distribution of HBIs in Southern Ocean surface sediments (Belt et al., 2016; Massé et al., 2011). The circum-Antarctic data set published by Belt et al. (2016), however, does not report HBI triene abundances. Significantly more studies so far focused on the use of $IPSO_{25}$ and the HBI Z-triene for paleo sea ice reconstructions and these records are commonly compared to micropaleontologial diatom analyses (e.g., Barbara et al., 2013; Collins et al., 2013; Denis et al., 2010).

Here, we provide a first overview of the distribution of $IPSO_{25}$, HBI trienes, brassicasterol and dinosterol in surface sediments from the northern part of the WAP (southern Drake Passage and Bransfield Strait). These biomarker data are completed by diatom analyses and remote sensing sea ice data. We further introduce and discuss the so-called $PIPSO_{25}$ index (phytoplankton-$IPSO_{25}$ index), which, following the PIP_{25} approach in the Arctic Ocean (Müller et al., 2011), may serve as a semi-quantitative indicator of past Southern Ocean sea ice cover. These biomarker-based sea ice estimates are compared to sea ice concentrations derived from diatom transfer functions and satellite-derived data on the recent sea ice conditions in the study area.

2 Oceanographic setting

The study area includes the southern Drake Passage and the Bransfield Strait located between the South Shetland Islands and the northern tip of the WAP (Fig. 2a and b). While the oceanographic setting in the Drake Passage is dominated by the Antarctic Circumpolar Current (ACC), a complex current system prevails in the Bransfield Strait. According to Sangrá et al. (2011) a branch of the ACC enters the Bransfield Strait in the west as the Bransfield Current, carrying transitional waters under the influence of the Bellingshausen Sea (Transitional Bellingshausen Sea Water, TBW). The TBW is characterized by a well-stratified, fresh and warm water mass with summer sea surface temperatures (SST) above 0° C. Below the shallow TBW, a narrow tongue of circumpolar deep water (CDW) flows along the slope of the South Shetland Islands (Sangrà et al., 2011). In the eastern part, transitional water from the Weddell Sea (Transitional Weddell Sea Water, TWW) enters the Bransfield Strait through the Antarctic Sound and from the Antarctic Peninsula (AP). This water mass corresponds to the Antarctic Coastal Current (Collares et al., 2018; Thompson et al., 2009). The TWW is significantly colder (summer SST < 0° C) and saltier due to extended sea ice formation in the Weddell Sea Gyre. The two water masses are separated at the sea surface by the Peninsula Front characterized by a TBW anticyclonic eddy system (Sangrà et al., 2011). While the TWW occupies the deep water column of the Bransfield Strait (Sangrà et al., 2011), it joins the surface TBW in the southwestern Bransfield Strait (Collares et al., 2018).

Due to high concentrations of dissolved iron on the shelf (Klunder et al., 2014), the area around the WAP is characterized by a high primary production with high vertical export fluxes during early summer associated with the formation of fast sinking mineral aggregates and fecal pellets (Kim et al., 2004; Wefer et al., 1988). The Peninsula Front divides the Bransfield Strait into two biogeographic regimes of high chlorophyll and diatom abundance in the TBW and low chlorophyll values and a pre-dominance of nanoplankton in the TWW (Gonçalves-Araujo et al., 2015), which is also reflected in the geochemistry of surface sediments (Cárdenas et al., 2018).

3 Materials and Methods

3.1 Sediment Samples and radiocarbon dating

In total, 26 surface sediment samples obtained by multicorers and box corers during the RV *Polarstern* cruise PS97 (Lamy, 2016) were analyzed (Fig. 2, Table 1). All samples were stored frozen and in glass vials. The composition of the sediments ranges from foraminiferal mud in the Drake Passage to diatomaceous mud with varying amounts of ice rafted debris in the Bransfield Strait (Lamy, 2016).

^{14}C radiocarbon dating of two samples from the PS97 cruise and one from the *Polarstern* cruise ANT-VI/2 (Fütterer, 1988) was conducted using the mini carbon dating system (MICADAS) at the Alfred Wegener Institute following the method of Wacker et al. (2010). The ^{14}C ages were calibrated to calendar years before present (cal BP) using the Calib 7.1 software (Stuiver et al., 2019) with an estimated reservoir age of 1178 years, derived from the six closest reference points listed in the Marine Reservoir Correction Database (www.calib.org).

3.2 Organic geochemical analyses

For biomarker analyses, sediments were freeze-dried and homogenized using an agate mortar. Also after freeze-drying, samples were stored frozen to avoid degradation. The extraction, purification and quantification of HBIs and sterols follow the analytical protocol applied by the international community of researchers performing HBI and sterol-based sea ice reconstructions (Belt et al., 2014; Stein et al., 2012). Prior to extraction, internal standards 7-hexylnonadecane (7-HND) and 5α-androstan-3β-ol were added to the sediments. For the ultrasonic extraction (15 min), a mixture of CH_2Cl_2:MeOH (v/v 2:1; 6ml) was added to the sediment. After centrifugation (2500 rpm for 1 min), the organic solvent layer was decanted. The ultrasonic extraction step was repeated twice. From the combined total organic extract, apolar hydrocarbons were separated via open column chromatography (SiO_2) using hexane (5 ml). Sterols were eluted with ethylacetate:hexane (v/v 20:80; 8 ml). HBIs were analyzed using an Agilent 7890B gas chromatography (30 m DB 1MS column, 0.25 mm diameter, 0.250 µm film thickness, oven temperature 60° C for 3 min, rise to 325° C within 23 min, holding 325° C for 16 min) coupled to an Agilent 5977B mass spectrometer (MSD, 70 eV constant ionization potential, ion source temperature 230° C). Sterols were first silylated (200 µl BSTFA; 60° C; 2hours) and then analyzed on the same instrument using a different oven temperature program (60° C for 2 min, rise to 150° C within 6 min, rise to 325° C within 56 min 40 sec). As recommended by Belt (2018), the identification of $IPSO_{25}$ and HBI trienes is based on comparison of their mass spectra with published mass spectra (Belt et al., 2000). Regarding the potential sulfurization of $IPSO_{25}$, we examined the GC-MS chromatogram and mass spectra of each sample for the occurrence of the HBI C_{25} sulfide (Sinninghe Damsté et al., 2007). The C_{25} HBI thiane was absent in all samples. For the quantification, manually

integrated peak areas of the molecular ions of the HBIs in relation to those of 7-HND were used. An external calibration for HBI diene and trienes was applied using a sample with known HBI concentrations from the Lancaster Sound, Canada, to account for the different response factors of the HBI molecular ions (m/z 346; m/z 348) and the fragment ion of 7-HND (m/z 266). The identification of sterols was based on comparison of their retention times and mass spectra with those of reference compounds run on the same instrument. Comparison of peak areas of individual analytes and the internal standard was used for sterol quantification. The error determined by duplicate GC-MS measurements was below 0.7%. The detection limit for HBIs and sterols was 0.5 ng/g sediment. Absolute concentrations of HBIs and sterols were normalized to total organic carbon contents (for TOC data see Cárdenas et al., 2018).

The herein presented phytoplankton-$IPSO_{25}$ index ($PIPSO_{25}$) is calculated using the same formula as for the PIP_{25} index following Müller et al. (2011):

$$PIPSO_{25} = \frac{IPSO_{25}}{IPSO_{25}+(c\times phytoplankton\ marker)} \quad (1)$$

The balance factor c (c = mean $IPSO_{25}$ / mean phytoplankton biomarker) is applied to account for the high offsets in the magnitude of $IPSO_{25}$ and sterol concentrations.

Stable carbon isotope composition of $IPSO_{25}$, requiring a minimum of 50 ng carbon, was successfully determined on five samples using GC-irm-MS. The ThermoFisher Scientific Trace GC was equipped with a 30m Restek Rxi-5 ms column (0.25 mm diameter, 0.25 µm film thickness) and coupled to a Finnigan MAT 252 isotope ratio mass spectrometer via a modified GC/C interface. Combustion of compounds was done under continuous flow in ceramic tubes filled with Ni wires at 1000° C under an oxygen trickle flow. The same GC program as for the HBI identification was used. The calibration was done by comparison to a CO_2 reference gas. The values of $\delta^{13}C$ are expressed in per mill (‰) against Vienna PeeDee Belemnite (VPDB) and the mean standard deviation was <0.9 ‰. An external standard mixture was measured every six runs, achieving a long-term mean standard deviation of 0.2‰ and an average accuracy of <0.1 ‰.

3.3 Diatoms

Details of the standard technique of diatom sample preparation were developed in the micropaleontological laboratory at the Alfred Wegener Institute (AWI) in Bremerhaven and described by Gersonde and Zielinski (2000). The counting procedure follows Schrader and Gersonde (1978) with a light microscope Zeiss Axioplan 2 at x1000 magnification.

Since *Chaetoceros* resting spores were highly abundant but not significant for diatom-based environmental analyses applied in this study they were not considered for sea ice calculations. To determine the transfer function

for the winter sea ice cover after Esper and Gersonde (2014a), most emphasis was given to the abundance and preservation of the sea ice indicative diatom species *Fragilariopsis curta* and *Fragilariopsis cylindrus*. Hereby, the general preservation state of the diatom assemblages was moderate to good in the Bransfield Strait and decreased towards the Drake Passage where it is moderate to poor. Cold water related diatom species known to dwell in the vicinity of sea ice, like *Thalassiosira weißflogii* and *Porosira pseudodenticulata* (Scott and Thomas, 2005), were also abundant (Table 4).

Diatoms species of *Fragilariopsis kerguelensis* but also A*zpeitia tabularis*, and *Thalassiosira lentiginosa* (and traces of *Thalassiosira oliverana*) were considered to reflect ice free habitats.

3.4 Sea ice data

The mean monthly satellite sea ice concentration was derived from Nimbus-7 SMMR and DMSP SSM/I-SSMIS passive microwave data and downloaded from the National Snow and Ice Data Center (NSIDC; Cavalieri et al., 1996). An interval from 1980 to 2015 was used to generate an average sea ice distribution for each season, spring (SON), summer (DJF), autumn (MAM) and winter (JJA).

4 Results and Discussion

4.1 Distribution of $IPSO_{25}$, HBI trienes and sterols

The sea ice biomarker $IPSO_{25}$ was detected in 14 samples, with concentrations ranging between 0.37 and 17.81 μg g^{-1} TOC (Table 1). The HBI Z-triene was present in all 26 samples (0.33-26.86 μg g^{-1} TOC) and the HBI E-triene was found in 24 samples (0.15-13.87 μg g^{-1} TOC). Brassicasterol was present in all measured samples with concentrations ranging from 3.39 to 5017.44 μg g^{-1} TOC while dinosterol was detected in 22 samples (0.0002-1983.75 μg g^{-1} TOC).

The distribution of $IPSO_{25}$ in the study area shows a clear northwest-southeast gradient (Fig. 3a) with concentrations increasing from the continental slope and around the South Shetland Islands towards the continental shelf. Maximum $IPSO_{25}$ concentrations are observed in the Bransfield Strait. According to Belt et al. (2016), deposition of $IPSO_{25}$ is highest in area covered by landfast sea ice and platelet ice during early spring and summer. We suppose that core sites PS97/068 to PS97/073 in the central and eastern Bransfield Strait are located too distal to be covered by fast ice and suggest that peak $IPSO_{25}$ concentrations at these sites may refer to the frequent drift and melt of sea ice exported from the Weddell Sea into the Bransfield Strait. The vertical export of biogenic material from sea ice towards the seafloor may be accelerated significantly by the formation of organic-mineral aggregates, fecal pellets or by (cryogenic) gypsum ballasting, which promotes a rapid burial and sedimentation of organic matter in polar settings (De La Rocha and Passow, 2007; Wefer et al., 1988; Wollenburg et al., 2018). Lateral subsurface advection of organic matter (incl. biomarkers) through the TWW, however, may also contribute to elevated $IPSO_{25}$ concentrations at these sites.

$IPSO_{25}$ was not detected in sediments from the permanently ice-free areas in the Drake Passage. Highest concentrations of both HBI trienes are found in the eastern Drake Passage and along the continental slope, while their concentrations in the Bransfield Strait are rather low (Fig. 3b and c) suggesting unfavorable environmental conditions (ocean temperature, sea ice cover) for their source diatoms.

We observe higher concentrations of brassicasterol and dinosterol in the eastern part of the Drake Passage and, in contrast to the observation made for HBI trienes, also in the eastern and central Bransfield Strait (Fig. 3d and e). Dinosterol and, in particular, brassicasterol are known to have different source organisms including diatoms, dinoflagellates, prymnesiophycean algae and cyanobacteria (Volkman, 1986) and we assume that this diversity may account for the higher concentration of these lipids in Bransfield Strait sediments, while concentrations of HBI trienes, mainly derived from diatoms, are significantly lower. Sediments collected along the Hero Fracture Zone in the western Drake Passage (Fig. 2) contain only minor amounts of biomarkers except for elevated brassicasterol concentrations observed at stations PS97/048-1 and 049-2 (Fig. 3d). This part of the Drake Passage

is mainly barren of fine-grained sediments and dominated by sands (Lamy, 2016), which may point to intensive winnowing by ocean currents impacting the deposition and burial of organic matter. We consider that also degradation of HBIs and sterols may affect their distribution within surface sediments. Rontani et al. (2014a) report a higher sensitivity of tri-unsaturated HBIs to oxidation but also note that oxidation conditions in pelagic environments (i.e. their source organisms' habitat) are not as significant as those within sea ice. A low reactivity towards oxidative degradation processes is observed for $IPSO_{25}$ (Rontani et al., 2014b, 2011), which supports the good preservation of this lipid in marine sediments. While these degradation studies are commonly conducted on laboratory diatom cultures and phytoplankton cell suspensions, investigations into degradation processes affecting both HBIs and sterols within sediments would address an important knowledge gap regarding in-situ biochemical modifications of the biomarker signal.

The $\delta^{13}C$ values of $IPSO_{25}$ are between -10.3‰ and -14.7‰ which is the commonly observed range for $IPSO_{25}$ in surface sediments and sea ice derived organic matter (Massé et al., 2011, Belt et al., 2016), and contrasts the low $\delta^{13}C$ values of marine phytoplankton lipids in Antarctic sediments (-38‰ to -41‰ after Massé et al., 2011).

Contrary to the finding of elevated Z-triene concentrations in surface waters along an ice-edge (Smik et al., 2016a) and earlier suggestions that this biomarker may be used as a proxy for MIZ conditions (Belt et al., 2015; Collins et al., 2013), we observe highest concentrations of the Z- and E-triene at the permanently ice-free northernmost stations in the eastern Drake Passage. This is also apparent for brassicasterol and dinosterol supporting an open marine (pelagic) source for these sterols. Moderate concentrations of HBI trienes at the continental slope along the WAP and in the Bransfield Strait likely refer to primary production at the sea ice margin during spring and summer indicating seasonal ice free waters in high production coastal areas influenced by upwelling (Gonçalves-Araujo et al., 2015). The similarity in the distribution of the Z- and the E-triene in our surface sediments – the latter of which so far is not often considered for Southern Ocean paleoenvironmental studies – supports the assumption of a common diatom source for these HBIs (Belt et al., 2000, 2017). Since brassicasterol and dinosterol are highly abundant in both seasonally ice covered Bransfield Strait sediments as well as in permanently ice-free Drake Passage sediments, their use as an indicator of fully open-marine conditions is questionable. Elevated concentrations of both sterols in the Bransfield Strait could either point to an additional input of these lipids from melting sea ice (Belt et al., 2013) or a better adaptation of some of their source organisms to cooler and/or ice-dominated ocean conditions. Production and accumulation of these lipids in (late) summer (i.e. after the sea ice season) may be considered as well. This observation highlights the need for a better understanding of the source organisms and the mechanisms involved in the synthesis of these sterols.

4.2 A novel sea ice index for the Southern Ocean: $PIPSO_{25}$

The main concept of combining the sea ice proxy with an indicator of an ice-free ocean environment (i.e. a phyotplankton biomarker, Müller et al., 2011), aims at a semi-quantitative assessment of the sea ice conditions. By reducing the light penetration through the ice, a thick and perennial sea ice cover limits the productivity of bottom sea ice algae (Hancke et al., 2018), which results in the absence of both, sea ice and pelagic phytoplankton biomarker lipids in the underlying sediments. Vice versa, sediments from permanently ice-free ocean areas only lack the sea ice biomarker but contain variable concentrations of phytoplankton biomarkers (Müller et al., 2011). The co-occurrence of both biomarkers in a sediment sample suggests seasonal sea ice coverage promoting algal production indicative of sea ice as well as open ocean environments (Müller et al., 2011).

Following the PIP_{25}-approach applied in the Arctic Ocean (Müller et al., 2011; Belt and Müller, 2013; Xiao et al., 2015) we used $IPSO_{25}$, HBI triene and sterol data to calculate the $PIPSO_{25}$ index. Depending on the biomarker reflecting pelagic (open ocean) conditions, we define P_ZIPSO_{25} (using the Z-triene), P_EIPSO_{25} (using the E-triene), P_BIPSO_{25} (using brassicasterol), and P_DIPSO_{25} (using dinosterol). Since the concentrations of $IPSO_{25}$ and both HBI trienes are in the same range, the application of the c-factor is not needed here. For the calculation of P_BIPSO_{25} the c-factor is 0.0048, for P_DIPSO_{25} it is 0.0137.

The $PIPSO_{25}$ values are 0 in the Drake Passage and increase to intermediate values at the South Shetland Islands and the continental slope and reach highest values in the Bransfield Strait (Fig. 4a-d). Minimum $PIPSO_{25}$ values are supposed to refer to a predominantly ice-free oceanic environment in the Drake Passage, while moderate $PIPSO_{25}$ values mark the transition towards a marginal sea ice coverage at the continental slope and around the South Shetland Islands. Elevated $PIPSO_{25}$ values in samples from the northeastern Bransfield Strait suggest an increased sea ice cover (probably sustained through the drift of sea ice originating in the Weddell Sea). This pattern reflects the oceanographic conditions of a permanently ice-free ocean north of the South Shetland Islands and a seasonal sea ice zone at the WAP influenced by the Weddell Sea as described by Cárdenas et al. (2018). Both HBI triene-based $PIPSO_{25}$ indices show constantly high values at the coast of the WAP of >0.7 (P_ZIPSO_{25}) and >0.8 (P_EIPSO_{25}), respectively, in the southern Bransfield Strait paralleling the southwest-northeast oriented Peninsula Front described by Sangrà et al. (2011). This front is reported to act as a barrier for phytoplankton communities (Gonçalves-Araujo et al., 2015) and is associated with the encounter between TWW carrying Weddell Sea sea ice through the Antarctic Sound and the TBW. The high $PIPSO_{25}$ values suggesting an extended sea ice cover west of the Peninsula Front (station PS97/054 and PS97/056) result from minimum concentrations of pelagic biomarkers and slightly higher concentrations of $IPSO_{25}$.

$PIPSO_{25}$ values based on the E-triene are about 0.2 higher compared to P_ZIPSO_{25}, due to the generally lower concentrations of the E-triene (Table 1). The sterol-based $PIPSO_{25}$ values display a generally similar pattern as $P_ZIPSO_{25}$and P_EIPSO_{25}, respectively, and we note a high comparability between the $P_EIPSO25$ and P_BIPSO_{25} values (r^2 = 0.73). Some differences, however, are observed in the southwestern part of the Bransfield Strait (station PS97/056) where P_BIPSO_{25} indicates a lower sea ice cover and in the central Bransfield Strait (stations PS97/068 and PS97/069) where P_BIPSO_{25} and P_DIPSO_{25} reflect only MIZ conditions. The HBI-triene based $PIPSO_{25}$ indices hence seem to reflect the oceanographic conditions within the Bransfield Strait more satisfactorily. We note that the brassicasterol or dinosterol-based $PIPSO_{25}$ index links environmental information derived from biomarker lipids belonging to different compound classes (i.e. HBIs and sterols), which have fundamentally different chemical properties. This requires special attention as, for example, selective degradation of one of the compounds may affect the sedimentary concentration of the respective lipids. Previous studies linking HBI and sterol-based sea ice reconstructions with satellite-derived or, with respect to downcore paleo studies, paleoclimatic data, however, demonstrate that the climatic/environmental conditions controlling the production of HBIs and sterols seem to exceed the influence of a potential preferential degradation of these biomarkers within the sediments (e.g., Berben et al., 2014; Cabedo-Sanz et al., 2013; Müller et al., 2009, 2012; Müller and Stein, 2014; Stein et al., 2017; Xiao et al., 2015). A comparison of PIP_{25} records determined using brassicasterol and the HBI Z-triene for three sediment cores from the Arctic realm covering the past up to 14.000 years BP (Belt et al., 2015) reveals very similar trends for both versions of the PIP_{25} index in each core, which may point to, at least, a similar degree of degradation of HBI trienes and sterols through time. More such studies are needed to evaluate the preservation potential of HBIs and sterols in Southern Ocean sediments.

4.3 Comparison of satellite-derived modern sea ice conditions and biomarker data

Satellite-derived sea ice data were averaged over the time period from 1980 to 2015 for all four seasons (Table 2) and are considered to reflect the modern mean state of sea ice coverage around the WAP. The sea ice concentration is expressed to range from 0 to 100 % and, although the error can be up to 15 %, concentrations below 15 % still suggest the occurrence of sea ice. These low sea ice concentrations are usually neglected for the determination of the sea ice extent, which is defined as the ocean area with a sea ice cover of at least 15 %. The spring and winter sea ice concentrations are shown in Figure 4 e-f. Winter sea ice is estimated to not extend north of 61° S (Fig. 4 f) and varies between 1 % and 50 % in the study area, while sea ice is reduced to less than 20 % in spring (Fig. 4e, Table 2).

Sea ice concentrations of up to 50 % are common in winter between the South Shetland Islands and north of the Antarctic Sound where the influence of TWW is highest. Permanent sea ice cover is uncommon in the Bransfield Strait and around the WAP and this area is mainly characterized by a high sea ice seasonality and drift ice from the Weddell Sea (Collares et al., 2018). Comparisons of individual biomarker concentrations with satellite sea ice data reveal a weak and positive correlation between $IPSO_{25}$ concentrations and winter sea ice concentrations (r^2 = 0.5), while no correlation is found between sea ice and pelagic biomarker concentrations ($r^2 < 0.1$ for all relations). Correlations of $PIPSO_{25}$ values with satellite-derived sea ice concentrations (for spring, summer, autumn and winter) contrast earlier observations made for the PIP_{25} index in the Arctic Ocean, where the closest linear relationship is found mainly with the spring sea ice coverage (i.e. the blooming season of sea ice algae; Müller et al., 2011; Xiao et al., 2015).

Esper and Gersonde (2014a) studied the response of diatom species to changes in environmental conditions and their response to the non-linear behaviour of sea ice dynamics (Zwally et al., 2002). In contrast to ice free areas or areas of permanent sea ice cover, areas characterized by the transition from consolidated to unconsolidated sea ice show rapid changes in satellite derived sea ice concentrations (ranging from 90 % to 15 %) and exhibit a large variability in species composition. To reflect this curve in sea ice we hence chose a cubic polynomial regression (polynomial of third degree) to determine the relation between $PIPSO_{25}$ values and satellite data depicting sea ice concentrations of more than 20 %.

We observe a remarkably low correlation between $PIPSO_{25}$ values and spring sea ice concentrations of less than 20 % with a coefficient of determination r^2 = 0.37 for P_ZIPSO_{25}, r^2 = 0.50 for P_EIPSO_{25} (Fig. 5a), r^2 = 0.31 for P_BIPSO_{25}, and r^2 = 0.34 for P_DIPSO_{25} (Fig. 5b). The highest correlation is observed between winter sea ice concentrations and P_EIPSO_{25} (r^2 = 0.72), and P_ZIPSO_{25} (r^2 = 0.65, Fig. 5c). A weaker correlation is noted for the sterol-based $PIPSO_{25}$ values (P_BIPSO_{25}: r^2 = 0.52; P_DIPSO_{25}: r^2 = 0.44, Fig. 5d). The slightly sigmoid-shaped regression line of winter sea ice concentrations and $PIPSO_{25}$ values reflects the non-linearity of sea ice cover in different sea ice regimes as mentioned above.

The contour lines in Figure 4 a-d show the observed extent of 15 %, 30 %, 40 % and 50 % winter sea ice compared to the $PIPSO_{25}$ values. In the northeastern part of the study area, the HBI triene based $PIPSO_{25}$ indices align well with the contour lines of winter sea ice concentrations and depict the gradient from the marginally ice-covered southern Drake Passage towards the intensively ice-covered Weddell Sea. In the southwestern part of the Bransfield Strait, all $PIPSO_{25}$ indices suggest a higher sea ice cover than it is reflected in the satellite data. This may be explained by the transport (and melt) of drift ice through the TWW, joining the TBW at the southwestern Peninsula Front. In contrast, also the absence of $IPSO_{25}$ at stations PS97/052 and PS97/053, off the continental

slope, is in conflict with the satellite data depicting an average winter sea ice cover of 23 %. Earlier documentations that the $IPSO_{25}$ producing sea ice diatom *Berkeleya adeliensis* favors land-fast ice communities in East Antarctica (Riaux-Gobin and Poulin, 2004) and platelet ice occurring mainly in near coastal areas (Belt et al., 2016) could explain this mismatch between biomarker and satellite data, which further strengthens the hypothesis that the application of $IPSO_{25}$ seems to be confined to continental shelf or near-coastal and meltwater affected environments (Belt et al., 2016). Alternatively, strong ocean currents (i.e. the ACC) could impact the deposition of $IPSO_{25}$ in this region.

As photosynthesis is not possible and a release of sea ice diatoms from melting sea ice is highly reduced during the Antarctic winter, the observation of a stronger correlation between recent winter sea ice concentrations and $PIPSO_{25}$ sea ice estimates is unexpected. We hence suggest that this offset may be related to the fact that the sediment samples integrate a longer time interval than is covered by satellite observations. Radiocarbon dating of selected samples that contain calcareous material reveals an age of 100 years BP in the vicinity of the South Shetland Islands (station PS97/059-2) and 142 years BP at the Antarctic Sound (station PS1546-2, Table 3). A significantly older age was determined for a sample of *N. pachyderma* from station PS97/044-1 (4830 years BP) in the Drake Passage. Bioturbation effects and uncertainties in reservoir ages potentially mask the ages of the near-coastal samples.

Nevertheless, since also other published ages of surface sediments within the Bransfield Strait (Barbara et al., 2013; Barnard et al., 2014; Etourneau et al., 2013; Heroy et al., 2008) are in the range of 0-270 years, we consider that our surface samples likely reflect the paleoenvironmental conditions that prevailed during the last two centuries (and not just the last 35 years covered by satellite observations). In the context of the rapid warming during the last century (Vaughan et al., 2003) and the decrease of sea ice at the WAP (King, 2014; King and Harangozo, 1998), we suggest that the biomarker data of the surface sediments relate to a spring sea ice cover, which must have been enhanced compared to the recent (past 35 years) spring sea ice recorded via remote sensing. Presumably, the average spring sea ice conditions over the past 200 years might have been similar to the modern (past 35 years) winter conditions, which would explain the stronger correlation between $PIPSO_{25}$ sea ice estimates and winter sea ice concentrations.

4.4 Comparison of diatom-based sea ice estimates and biomarker data

The diatoms preserved in sediments from the study area (Table 4) can be associated with open ocean and sea ice conditions. North of the South Shetland Islands, the strong influence of the ACC is reflected in the high abundance of open ocean diatom species such as *Fragilariopsis kerguelensis* and *Thalassiosira lentiginosa* (Esper et al.,

2010). The two diatom species *Fragilariopsis curta* and *Fragilariopsis cylindrus* – known to not produce HBI (Belt et al., 2016; Sinninghe Damsté et al., 2004) – are used for the reconstruction of sea ice conditions (Gersonde and Zielinski, 2000; Xiao et al., 2016). They mark the vicinity to sea ice (Buffen et al., 2007; Pike et al., 2008) and indicate fast and melting ice, a stable sea ice margin and stratification due to melting processes and the occurrence of seasonal sea ice. The high abundance of these species in our samples is in good agreement with high and moderate $IPSO_{25}$ concentrations and $PIPSO_{25}$ values in the Bransfield Strait and around the South Shetland Islands, respectively. The only HBI source diatom identified is the HBI Z-triene producing *Rhizosolenia hebetata* (Belt et al., 2017), which is present in four samples in rather small amounts and does not show a relation to the measured Z-triene concentrations (Table 1 and 4). The source diatom of $IPSO_{25}$ *Berkeleya adeliensis* was not observed (or preserved) in the samples, and we assume that other, hitherto unknown, producers may exist.

We applied the transfer function of Esper and Gersonde (2014a) with four analogs (4an, Table 4) to our samples to compare the different estimates of sea ice cover based on biomarkers and diatoms. A positive correlation of the linear relationship is found between winter sea ice (WSI) concentrations derived from diatoms and the $PIPSO_{25}$ indices based on HBI trienes (P_ZIPSO_{25} with $r^2 = 0.76$; P_EIPSO_{25} with $r^2 = 0.77$, Fig. 6a). The correlations of sterol-based $PIPSO_{25}$ values with WSI are slightly lower but in the same range (P_BIPSO_{25} with $r^2 = 0.74$; P_DIPSO_{25} with $r^2 = 0.69$, Fig. 6b). A slightly weaker correlation is noted for diatom- and satellite-based winter sea ice concentrations ($r^2 = 0.63$; Fig. 6c). Overall, the diatom approach indicates higher sea ice concentrations than the satellite data with an offset of up to 65 %. This may be due to different sources of satellite reference data used for the transfer function or also due to the fact that the sediment samples integrate a longer time period with a higher sea ice cover than the satellite data (see discussion in section 4.3).

4.5 Application of $PIPSO_{25}$ as a semi-quantitative sea ice index

Precise and, in particular, quantitative reconstructions of past sea ice coverage are crucial for a robust assessment of feedback mechanisms in the ice-ocean-atmosphere system. While diatom transfer functions provide a valuable tool, additional information on sea ice conditions in coastal ice-shelf proximal areas, which are often affected by opal dissolution, are essential. The $PIPSO_{25}$ approach seems to be a promising step into this direction, though our data obtained for the WAP are not yet sufficient for a full calibration. $PIPSO_{25}$, diatom and satellite sea ice data, however, reveal positive correlations (Figs. 5 and 6) and depict similar gradients in sea ice cover. The observed offset between satellite data and biomarker- and diatom-based sea ice estimates likely relates to the fact that the instrumental records cover a significantly shorter or more recent time interval than the studied sediments. The recent rapid warming along the WAP (Vaughan et al., 2003) hence complicates attempts to calibrate these proxy

data against observational data. The high correlation between diatom-derived winter sea ice concentrations and $PIPSO_{25}$ values (Fig. 6a and b) may even argue for a calibration of the $IPSO_{25}$ index against diatom data. The robustness and reliability of such an approach, however, has to be proven by means of a larger data set. Regarding the interpretation of $PIPSO_{25}$ in terms of sea ice coverage in the study area, lower $PIPSO_{25}$ values (<0.15 for P_ZIPSO_{25}; <0.31 for P_EIPSO_{25}; <0.22 for P_BIPSO_{25} and P_DIPSO_{25}) roughly seem to reflect unconsolidated, drifting winter sea ice and a nearly ice-free spring season. Higher values (>0.71 for P_ZIPSO_{25}; >0.9 P_EIPSO_{25}; >0.6 for P_BIPSO_{25} and P_DIPSO_{25}) would refer to an extended winter sea ice cover (up to 91 % in some years) with ice floes remaining until summer.

5 Conclusion

The distribution of the sea ice biomarker $IPSO_{25}$ and related HBI trienes and sterols as well as diatoms in a suite of surface sediments from the southern Drake Passage and the WAP reflects recent sea ice conditions reasonably well. The herein proposed sea ice index $PIPSO_{25}$ indicates seasonal sea ice cover along the coast of the WAP and in the Bransfield Strait, whereas mainly ice-free conditions prevail in the Drake Passage. In general, this pattern is consistent with satellite-derived sea ice data and diatom-based sea ice estimates and we note that the $PIPSO_{25}$ index seems a promising approach towards semi-quantitative sea ice reconstructions in the Southern Ocean. The recent rapid warming in the study area, however, affects the comparability of proxy and satellite data. The fact that the surface sediments integrate a significantly longer time interval than the remote sensing data thwarts attempts to calibrate $PIPSO_{25}$ values against observed sea ice concentrations. Additional data from other circum-Antarctic coastal (and distal) environments and investigations into potential calibration methods are needed to further develop this index as a quantitative sea ice proxy.

Data Availability

All data can be found in this paper and will be available at the open access repository *www.pangaea.de*.

Author contributions

The study was conceived by MV and JM. Data collections and experimental investigations were done by MV together with OE (diatoms), GM (radiocarbon dating), CH (satellite data), and ES (isotope data). MV wrote the manuscript and did the visualizations. KF provided technical support. JM supervised the study. All authors contributed to the interpretation and discussion of the results and the conclusion of this study.

Competing interests

None of the authors has a conflict of interest.

Acknowledgement

We thank the captain and crew of RV Polarstern cruise PS97, and the following supporters: Mandy Kiel (technician), Lester Lembke-Jene (biology, dating), Liz Bonk and Hendrik Grotheer (from MICADAS), Max Mues (sample preparation), Nicoletta Ruggieri (lab support), Walter Luttmer (lab support). Simon Belt is acknowledged for providing the 7-HND internal standard for HBI quantification. Financial support was provided through the Helmholtz Research grant VH-NG-1101.

References

Arrigo, K. R., Worthen, D. L., Lizotte, M. P., Dixon, P. and Dieckmann, G.: Primary Production in Antarctic Sea Ice, Science, 276, 394–397, doi:10.1126/science.276.5311.394, 1997.

Barbara, L., Crosta, X., Schmidt, S. and Massé, G.: Diatoms and biomarkers evidence for major changes in sea ice conditions prior the instrumental period in Antarctic Peninsula, Quat. Sci. Rev., 79, 99–110, doi:10.1016/j.quascirev.2013.07.021, 2013.

Barbara, L., Crosta, X., Leventer, A., Schmidt, S., Etourneau, J., Domack, E. and Massé, G.: Environmental responses of the Northeast Antarctic Peninsula to the Holocene climate variability, Paleoceanography, 31(1), 131–147, doi:10.1002/2015PA002785, 2016.

Bárcena, M. A., Gersonde, R., Ledesma, S., Fabrés, J., Calafat, A. M., Canals, M., Sierro, F. J. and Flores, J. A.: Record of Holocene glacial oscillations in Bransfield Basin as revealed by siliceous microfossil assemblages, Antarct. Sci., 10(03), 269–285, doi:10.1017/S0954102098000364, 1998.

Barnard, A., Wellner, J. S. and Anderson, J. B.: Late Holocene climate change recorded in proxy records from a Bransfield Basin sediment core, Antarctic Peninsula, Polar Res., 33(1), doi:10.3402/polar.v33.17236, 2014.

Belt, S. T.: Source-specific biomarkers as proxies for Arctic and Antarctic sea ice, Org. Geochem., 125, 277–298, doi:10.1016/j.orggeochem.2018.10.002, 2018.

Belt, S. T. and Müller, J.: The Arctic sea ice biomarker IP 25 : a review of current understanding , recommendations for future research and applications in palaeo sea ice reconstructions, Quat. Sci. Rev., 79, 9–25, doi:10.1016/j.quascirev.2012.12.001, 2013.

Belt, S. T., Allard, W. G., Massé, G., Robert, J. M. and Rowland, S. J.: Highly branched isoprenoids (HBIs): Identification of the most common and abundant sedimentary isomers, Geochim. Cosmochim. Acta, 64(22), 3839–3851, doi:10.1016/S0016-7037(00)00464-6, 2000.

Belt, S. T., Masse, G., Rowland, S. J., Poulin, M., Michel, C. and Leblanc, B.: A novel chemical fossil of palaeo sea ice : IP 25, Org. Geochem., 38, 16–27, doi:10.1016/j.orggeochem.2006.09.013, 2007.

Belt, S. T., Brown, T. A., Ringrose, A. E., Cabedo-Sanz, P., Mundy, C. J., Gosselin, M. and Poulin, M.: Quantitative measurement of the sea ice diatom biomarker IP25 and sterols in Arctic sea ice and underlying sediments: Further considerations for palaeo sea ice reconstruction, Org. Geochem., 62, 33–45, doi:10.1016/J.ORGGEOCHEM.2013.07.002, 2013.

Belt, S. T., Brown, T. A., Ampel, L., Cabedo-Sanz, P., Fahl, K., Kocis, J. J., Massé, G., Navarro-Rodriguez, A., Ruan,

J. and Xu, Y.: An inter-laboratory investigation of the Arctic sea ice biomarker proxy IP₂₅ in marine sediments: key outcomes and recommendations, Clim. Past, 10(1), 155–166, doi:10.5194/cp-10-155-2014, 2014.

Belt, S. T., Cabedo-Sanz, P., Smik, L., Navarro-Rodriguez, A., Berben, S. M. P., Knies, J. and Husum, K.: Identification of paleo Arctic winter sea ice limits and the marginal ice zone: Optimised biomarker-based reconstructions of late Quaternary Arctic sea ice, Earth Planet. Sci. Lett., 431, 127–139, doi:10.1016/j.epsl.2015.09.020, 2015.

Belt, S. T., Smik, L., Brown, T. A., Kim, J. H., Rowland, S. J., Allen, C. S., Gal, J. K., Shin, K. H., Lee, J. I. and Taylor, K. W. R.: Source identification and distribution reveals the potential of the geochemical Antarctic sea ice proxy IPSO25, Nat. Commun., 7, 1–10, doi:10.1038/ncomms12655, 2016.

Belt, S. T., Brown, T. A., Smik, L., Tatarek, A., Wiktor, J., Stowasser, G., Assmy, P., Allen, C. S. and Husum, K.: Identification of C25 highly branched isoprenoid (HBI) alkenes in diatoms of the genus Rhizosolenia in polar and sub-polar marine phytoplankton, Org. Geochem., 110, 65–72, doi:10.1016/j.orggeochem.2017.05.007, 2017.

Belt, S. T., Brown, T. A., Smik, L., Assmy, P. and Mundy, C. J.: Sterol identification in floating Arctic sea ice algal aggregates and the Antarctic sea ice diatom Berkeleya adeliensis, Org. Geochem., 118, 1–3, doi:10.1016/j.orggeochem.2018.01.008, 2018.

Berben, S. M. P., Husum, K., Cabedo-Sanz, P. and Belt, S. T.: Holocene sub-centennial evolution of Atlantic water inflow and sea ice distribution in the western Barents Sea, Clim. Past, 10(1), 181–198, doi:10.5194/cp-10-181-2014, 2014.

Buffen, A., Leventer, A., Rubin, A. and Hutchins, T.: Diatom assemblages in surface sediments of the northwestern Weddell Sea, Antarctic Peninsula, Mar. Micropaleontol., 62(1), 7–30, doi:10.1016/J.MARMICRO.2006.07.002, 2007.

Burckle, L. H. and Cooke, D. W.: Late Pleistocene Eucampia antarctica Abundance Stratigraphy in the Atlantic Sector of the Southern Ocean, Micropaleontology, 29(1), 6, doi:10.2307/1485648, 1983.

Cabedo-Sanz, P., Belt, S. T., Knies, J. and Husum, K.: Identification of contrasting seasonal sea ice conditions during the Younger Dryas, Quat. Sci. Rev., 79, 74–86, doi:10.1016/j.quascirev.2012.10.028, 2013.

Cárdenas, P., Lange, C. B., Vernet, M., Esper, O., Srain, B., Vorrath, M.-E., Ehrhardt, S., Müller, J., Kuhn, G., Arz, H. W., Lembke-Jene, L. and Lamy, F.: Biogeochemical proxies and diatoms in surface sediments across the Drake Passage reflect oceanic domains and frontal systems in the region, Prog. Oceanogr.,

doi:10.1016/j.pocean.2018.10.004, 2018.

Cavalieri, D. J., Parkinson, C. L., Gloersen, P. and Zwally, H. J.: Sea Ice Concentrations from Nimbus-7 SMMR and DMSP SSM/I-SSMIS Passive Microwave Data, Version 1, Boulder, Color. USA, doi:10.5067/8GQ8LZQVL0VL, 1996.

Collares, L. L., Mata, M. M., Kerr, R., Arigony-Neto, J. and Barbat, M. M.: Iceberg drift and ocean circulation in the northwestern Weddell Sea, Antarctica, Deep Sea Res. Part II Top. Stud. Oceanogr., 149(January 2019), 10–24, doi:10.1016/j.dsr2.2018.02.014, 2018.

Collins, L. G., Allen, C. S., Pike, J., Hodgson, D. A., Weckström, K. and Massé, G.: Evaluating highly branched isoprenoid (HBI) biomarkers as a novel Antarctic sea-ice proxy in deep ocean glacial age sediments, Quat. Sci. Rev., 79, 87–98, doi:10.1016/j.quascirev.2013.02.004, 2013.

Crosta, X., Pichon, J.-J. and Burckle, L. H.: Application of modern analog technique to marine Antarctic diatoms: Reconstruction of maximum sea-ice extent at the Last Glacial Maximum, Paleoceanography, 13(3), 284–297, doi:10.1029/98PA00339, 1998.

De La Rocha, C. L. and Passow, U.: Factors influencing the sinking of POC and the efficiency of the biological carbon pump, Deep Sea Res. Part II Top. Stud. Oceanogr., 54(5–7), 639–658, doi:10.1016/j.dsr2.2007.01.004, 2007.

Denis, D., Crosta, X., Barbara, L., Massé, G., Renssen, H., Ther, O. and Giraudeau, J.: Sea ice and wind variability during the Holocene in East Antarctica: insight on middle–high latitude coupling, Quat. Sci. Rev., 29(27–28), 3709–3719, doi:10.1016/J.QUASCIREV.2010.08.007, 2010.

Esper, O. and Gersonde, R.: New tools for the reconstruction of Pleistocene Antarctic sea ice, Palaeogeogr. Palaeoclimatol. Palaeoecol., 399, 260–283, doi:10.1016/J.PALAEO.2014.01.019, 2014a.

Esper, O. and Gersonde, R.: Quaternary surface water temperature estimations: New diatom transfer functions for the Southern Ocean, Palaeogeogr. Palaeoclimatol. Palaeoecol., 414, 1–19, doi:10.1016/J.PALAEO.2014.08.008, 2014b.

Esper, O., Gersonde, R. and Kadagies, N.: Diatom distribution in southeastern Pacific surface sediments and their relationship to modern environmental variables, Palaeogeogr. Palaeoclimatol. Palaeoecol., 287(1–4), 1–27, doi:10.1016/J.PALAEO.2009.12.006, 2010.

Etourneau, J., Collins, L. G., Willmott, V., Kim, J. H., Barbara, L., Leventer, A., Schouten, S., Sinninghe Damsté, J. S., Bianchini, A., Klein, V., Crosta, X. and Massé, G.: Holocene climate variations in the western Antarctic

Peninsula: Evidence for sea ice extent predominantly controlled by changes in insolation and ENSO variability, Clim. Past, 9(4), 1431–1446, doi:10.5194/cp-9-1431-2013, 2013.

Fütterer, D. K.: Die Expedition ANTARKTIS-VI mit FS Polarstern 1987/1988 (The Expedition ANTARKTIS-VI of RV Polarstern in 1987/88), Alfred-Wegener-Institut für Polar- und Meeresforschung, Bremerhaven, Germany., 1988.

Gersonde, R. and Zielinski, U.: The reconstruction of late Quaternary Antarctic sea-ice distribution — the use of diatoms as a proxy for sea-ice, Palaeogeogr. Palaeoclimatol. Palaeoecol., 162, 263–286, doi:10.1016/S0031-0182(00)00131-0, 2000.

Gonçalves-Araujo, R., de Souza, M. S., Tavano, V. M. and Garcia, C. A. E.: Influence of oceanographic features on spatial and interannual variability of phytoplankton in the Bransfield Strait, Antarctica, J. Mar. Syst., 142, 1–15, doi:10.1016/J.JMARSYS.2014.09.007, 2015.

Hancke, K., Lund-Hansen, L. C., Lamare, M. L., Højlund Pedersen, S., King, M. D., Andersen, P. and Sorrell, B. K.: Extreme Low Light Requirement for Algae Growth Underneath Sea Ice: A Case Study From Station Nord, NE Greenland, J. Geophys. Res. Ocean., 123(2), 985–1000, doi:10.1002/2017JC013263, 2018.

Heroy, D. C., Sjunneskog, C. and Anderson, J. B.: Holocene climate change in the Bransfield Basin, Antarctic Peninsula: evidence from sediment and diatom analysis, Antarct. Sci., 20(01), 69–87, doi:10.1017/S0954102007000788, 2008.

Hobbs, W. R., Massom, R., Stammerjohn, S., Reid, P., Williams, G. and Meier, W.: A review of recent changes in Southern Ocean sea ice , their drivers and forcings, Glob. Planet. Change, 143, 228–250, doi:10.1016/j.gloplacha.2016.06.008, 2016.

Hofmann, E. E., Klinck, J. M., Lascara, C. M. and Smith, D. A.: Water mass distribution and circulation west of the Antarctic Peninsula and including Bransfield Strait, in Foundations for Ecological Research West of the Antarctic Peninsula, edited by R. . Ross, E. E. Hofmann, and L. B. Quetin, pp. 61–80, American Geophysical Union (AGU), Washington, D. C., 1996.

Kanazawa, A., Yoshioka, M. and Teshima, S.-I.: The occurrence of brassicasterol in the diatoms, Cyclotella nana and Nitzschia closterium, Bull. Japanese Soc. Sci. Fish., 37, 889–903, 1971.

Kim, D., Kim, D. Y., Kim, Y. J., Kang, Y. C. and Shim, J.: Downward fluxes of biogenic material in Bransfield Strait, Antarctica, Antarct. Sci., 16(3), 227–237, doi:10.1017/S0954102004002032, 2004.

King, J.: A resolution of the Antarctic paradox, Nature, 505(7484), 491–492, doi:10.1038/505491a, 2014.

King, J. C. and Harangozo, S. A.: Climate change in the western Antarctic Peninsula since 1945: observations and possible causes, Ann. Glaciol., 27, 571–575, doi:10.3189/1998AoG27-1-571-575, 1998.

Klunder, M. B., Laan, P., De Baar, H. J. W., Middag, R., Neven, I. and Van Ooijen, J.: Dissolved Fe across the Weddell Sea and Drake Passage: impact of DFe on nutrient uptake, Biogeosciences, 11(3), 651–669, doi:10.5194/bg-11-651-2014, 2014.

Lamy, F.: The expedition PS97 of the research vessel POLARSTERN to the Drake Passage in 2016, Reports Polar Mar. Res., 7'01, 1–571, doi:10.2312/BzPM_0702_2016, 2016.

Leventer, A.: The fate of Antarctic "sea ice diatoms" and their use as paleoenvironmental indicators, in Antarctic Research Series, edited by M. P. Lizotte and K. R. Arrigo, pp. 121–137, American Geophysical Union (AGU)., 1998.

Liu, J., Curry, J. A. and Martinson, D. G.: Interpretation of recent Antarctic sea ice variability, Geophys. Res. Lett., 31(2), 2000–2003, doi:10.1029/2003GL018732, 2004.

Massé, G., Belt, S. T., Crosta, X., Schmidt, S., Snape, I., Thomas, D. N. and Rowland, S. J.: Highly branched isoprenoids as proxies for variable sea ice conditions in the Southern Ocean, Antarct. Sci., 23(05), 487–498, doi:10.1017/S0954102011000381, 2011.

Minzoni, R. T., Anderson, J. B., Fernandez, R. and Wellner, J. S.: Marine record of Holocene climate, ocean, and cryosphere interactions: Herbert Sound, James Ross Island, Antarctica, Quat. Sci. Rev., 129, 239–259, doi:10.1016/j.quascirev.2015.09.009, 2015.

Morrison, A. K., England, M. H. and Hogg, A. M.: Response of Southern Ocean Convection and Abyssal Overturning to Surface Buoyancy Perturbations, J. Clim., 28(10), 4263–4278, doi:10.1175/JCLI-D-14-00110.1, 2015.

Müller, J. and Stein, R.: High-resolution record of late glacial and deglacial sea ice changes in Fram Strait corroborates ice–ocean interactions during abrupt climate shifts, Earth Planet. Sci. Lett., 403, 446–455, doi:10.1016/j.epsl.2014.07.016, 2014.

Müller, J., Massé, G., Stein, R. and Belt, S. T.: Variability of sea-ice conditions in the Fram Strait over the past 30,000 years, Nat. Geosci., 2(11), 772–776, doi:10.1038/ngeo665, 2009.

Müller, J., Wagner, A., Fahl, K., Stein, R., Prange, M. and Lohmann, G.: Towards quantitative sea ice reconstructions in the northern North Atlantic: A combined biomarker and numerical modelling approach, Earth Planet. Sci. Lett., 306(3–4), 137–148, doi:10.1016/J.EPSL.2011.04.011, 2011.

Müller, J., Werner, K., Stein, R., Fahl, K., Moros, M. and Jansen, E.: Holocene cooling culminates in sea ice oscillations in Fram Strait, Quat. Sci. Rev., 47, 1–14, doi:10.1016/j.quascirev.2012.04.024, 2012.

Nichols, P. D., Volkman, J. K., Palmisano, A. C., Smith, G. A. and White, D. C.: Occurrence of an Isoprenoid C25 diunsaturated alkene and high neutral lipid content in Antarctic Sea-Ice Diatom communities, J. Phycol., 24, 90–96, 1988.

Orsi, A. H., Smethie, W. M. and Bullister, J. L.: On the total input of Antarctic waters to the deep ocean: A preliminary estimate from chlorofluorocarbon measurements, J. Geophys. Res., 107, 31-, doi:10.1029/2001JC000976, 2002.

Parkinson, C. L.: Trends in the length of the Southern Ocean sea-ice season, 1979-99, Ann. Glaciol., 34(1), 435–440, doi:10.3189/172756402781817482, 2002.

Parkinson, C. L. and Cavalieri, D. J.: Antarctic sea ice variability and trends, 1979–2010, Cryosph., 6, 871–880, doi:10.5194/tc-6-871-2012, 2012.

Pike, J., Allen, C. S., Leventer, A., Stickley, C. E. and Pudsey, C. J.: Comparison of contemporary and fossil diatom assemblages from the western Antarctic Peninsula shelf, Mar. Micropaleontol., 67(3–4), 274–287, doi:10.1016/J.MARMICRO.2008.02.001, 2008.

Ragueneau, O., Tréguer, P., Leynaert, A., Anderson, R. ., Brzezinski, M. ., DeMaster, D. ., Dugdale, R. ., Dymond, J., Fischer, G., François, R., Heinze, C., Maier-Reimer, E., Martin-Jézéquel, V., Nelson, D. . and Quéguiner, B.: A review of the Si cycle in the modern ocean: recent progress and missing gaps in the application of biogenic opal as a paleoproductivity proxy, Glob. Planet. Change, 26(4), 317–365, doi:10.1016/S0921-8181(00)00052-7, 2000.

Riaux-Gobin, C. and Poulin, M.: Possible symbiosis of Berkeleya adeliensis Medlin, Synedropsis fragilis (Manguin) Hasle et al. and Nitzschia lecointei Van Heurck (bacillariophyta) associated with land-fast ice in Adélie Land, Antarctica, Diatom Res., 19(2), 265–274, doi:10.1080/0269249X.2004.9705874, 2004.

Rintoul, S. R.: Rapid freshening of Antarctic Bottom Water formed in the Indian and Pacific oceans, Geophys. Res. Lett., 34(6), L06606, doi:10.1029/2006GL028550, 2007.

Rontani, J.-F., Belt, S. T., Vaultier, F., Brown, T. A. and Massé, G.: Autoxidative and Photooxidative Reactivity of Highly Branched Isoprenoid (HBI) Alkenes, Lipids, 49(5), 481–494, doi:10.1007/s11745-014-3891-x, 2014a.

Rontani, J.-F., Belt, S. T., Brown, T. A., Vaultier, F. and Mundy, C. J.: Sequential photo- and autoxidation of diatom lipids in Arctic sea ice, Org. Geochem., 77, 59–71, doi:10.1016/j.orggeochem.2014.09.009, 2014b.

Rontani, J. F., Belt, S. T., Vaultier, F. and Brown, T. A.: Visible light induced photo-oxidation of highly branched

1 isoprenoid (HBI) alkenes: Significant dependence on the number and nature of double bonds, Org. Geochem.,
2 42(7), 812–822, doi:10.1016/j.orggeochem.2011.04.013, 2011.
3 Sangrà, P., Gordo, C., Hernández-Arencibia, M., Marrero-Díaz, A., Rodríguez-Santana, A., Stegner, A., Martínez-
4 Marrero, A., Pelegrí, J. L. and Pichon, T.: The Bransfield current system, Deep Sea Res. Part I Oceanogr. Res.
5 Pap., 58(4), 390–402, doi:10.1016/J.DSR.2011.01.011, 2011.
6 Schrader, H. and Gersonde, R.: Diatoms and silicoflagellates, in Micropaleontological Methods and Techniques -
7 An Excercise on an Eight Meter Section of the Lower Pliocene of Capo Rossello, Sicily, Utrecht
8 Micropaleontological Bulletins, vol. 17, edited by W. J. Zachariasse, W. R. Riedel, A. Sanfilippo, R. R. Schmidt, M.
9 J. Brolsma, H. J. Schrader, R. Gersonde, M. M. Drooger, and J. A. Broekman, pp. 129–176., 1978.
10 Scott, F. J. and Thomas, D. P.: Diatoms, in Antarctic Marine Protists, p. 563, Australian Biological Resources
11 Study, Canberra & Hobart., 2005.
12 Sinninghe Damsté, J. S., Muyzer, G., Abbas, B., Rampen, S. W., Massé, G., Allard, W. G., Belt, S. T., Robert, J. M.,
13 Rowland, S. J., Moldowan, J. M., Barbanti, S. M., Fago, F. J., Denisevich, P., Dahl, J., Trindade, L. A. F. and
14 Schouten, S.: The Rise of the Rhizosolenid Diatoms, Science (80-.)., 304(5670), 584–587,
15 doi:10.1126/science.1096806, 2004.
16 Sinninghe Damsté, J. S., Rijpstra, W. I. C., Coolen, M. J. L., Schouten, S. and Volkman, J. K.: Rapid sulfurisation of
17 highly branched isoprenoid (HBI) alkenes in sulfidic Holocene sediments from Ellis Fjord, Antarctica, Org.
18 Geochem., 38(1), 128–139, doi:10.1016/j.orggeochem.2006.08.003, 2007.
19 Smik, L., Belt, S. T., Lieser, J. L., Armand, L. K. and Leventer, A.: Distributions of highly branched isoprenoid
20 alkenes and other algal lipids in surface waters from East Antarctica: Further insights for biomarker-based
21 paleo sea-ice reconstruction, Org. Geochem., 95, 71–80, doi:10.1016/J.ORGGEOCHEM.2016.02.011, 2016a.
22 Smik, L., Cabedo-Sanz, P. and Belt, S. T.: Semi-quantitative estimates of paleo Arctic sea ice concentration
23 based on source-specific highly branched isoprenoid alkenes: A further development of the PIP 25 index, Org.
24 Geochem., 92, 63–69, doi:10.1016/j.orggeochem.2015.12.007, 2016b.
25 Stein, R., Fahl, K. and Müller, J.: Proxy Reconstruction of Cenozoic Arctic Ocean Sea-Ice History: from IRD to
26 IP25, Polarforschung, 82(1), 37–71, 2012.
27 Stein, R., Fahl, K., Gierz, P., Niessen, F. and Lohmann, G.: Arctic Ocean sea ice cover during the penultimate
28 glacial and the last interglacial, Nat. Commun., 8(1), 373, doi:10.1038/s41467-017-00552-1, 2017.
29 Stuiver, M., Reimer, P. J. and Reimer, R. W.: Calib 7.1, [online] Available from: http://calib.org, 2019.

Thompson, A. F., Heywood, K. J., Thorpe, S. E., Renner, A. H. H. and Trasviña, A.: Surface Circulation at the Tip of the Antarctic Peninsula from Drifters, J. Phys. Oceanogr., 39(1), 3–26, doi:10.1175/2008JPO3995.1, 2009.

Vaughan, D. G., Marshall, G. J., Connolley, W. M., Parkinson, C., Mulvaney, R., Hodgson, D. A., King, J. C., Pudsey, C. J. and Turner, J.: Recent Rapid Regional Climate Warming on the Antarctic Peninsula, Clim. Change, 60(3), 243–274, doi:10.1023/A:1026021217991, 2003.

Volkman, J. K.: A review of sterol markers for marine and terrigenous organic matter, Org. Geochem., 9(2), 83–99, doi:10.1016/0146-6380(86)90089-6, 1986.

Volkman, J. K.: Sterols in microorganisms, Appl. Microbiol. Biotechnol., 60(5), 495–506, doi:10.1007/s00253-002-1172-8, 2003.

Wacker, L., Bonani, G., Friedrich, M., Hajdas, I., Kromer, B., Němec, M., Ruff, M., Suter, M., Synal, H.-A. and Vockenhuber, C.: MICADAS: Routine and High-Precision Radiocarbon Dating, Radiocarbon, 52(02), 252–262, doi:10.1017/S0033822200045288, 2010.

Wefer, G., Fischer, G., Füetterer, D. and Gersonde, R.: Seasonal particle flux in the Bransfield Strait, Antartica, Deep Sea Res. Part A. Oceanogr. Res. Pap., 35(6), 891–898, doi:10.1016/0198-0149(88)90066-0, 1988.

Wollenburg, J. E., Katlein, C., Nehrke, G., Nöthig, E.-M., Matthiessen, J., Wolf- Gladrow, D. A., Nikolopoulos, A., Gázquez-Sanchez, F., Rossmann, L., Assmy, P., Babin, M., Bruyant, F., Beaulieu, M., Dybwad, C. and Peeken, I.: Ballasting by cryogenic gypsum enhances carbon export in a Phaeocystis under-ice bloom, Sci. Rep., 8(1), 7703, doi:10.1038/s41598-018-26016-0, 2018.

Xiao, W., Esper, O. and Gersonde, R.: Last Glacial - Holocene climate variability in the Atlantic sector of the Southern Ocean, Quat. Sci. Rev., 135, 115–137, doi:10.1016/j.quascirev.2016.01.023, 2016.

Xiao, X., Fahl, K., Müller, J. and Stein, R.: Sea-ice distribution in the modern Arctic Ocean: Biomarker records from trans-Arctic Ocean surface sediments, Geochim. Cosmochim. Acta, 155, 16–29, doi:10.1016/J.GCA.2015.01.029, 2015.

Zwally, H. J., Comiso, J. C., Parkinson, C. L., Cavalieri, D. J. and Gloersen, P.: Variability of Antarctic sea ice 1979–1998, J. Geophys. Res., 107(C5), 3041, doi:10.1029/2000JC000733, 2002.

Figures

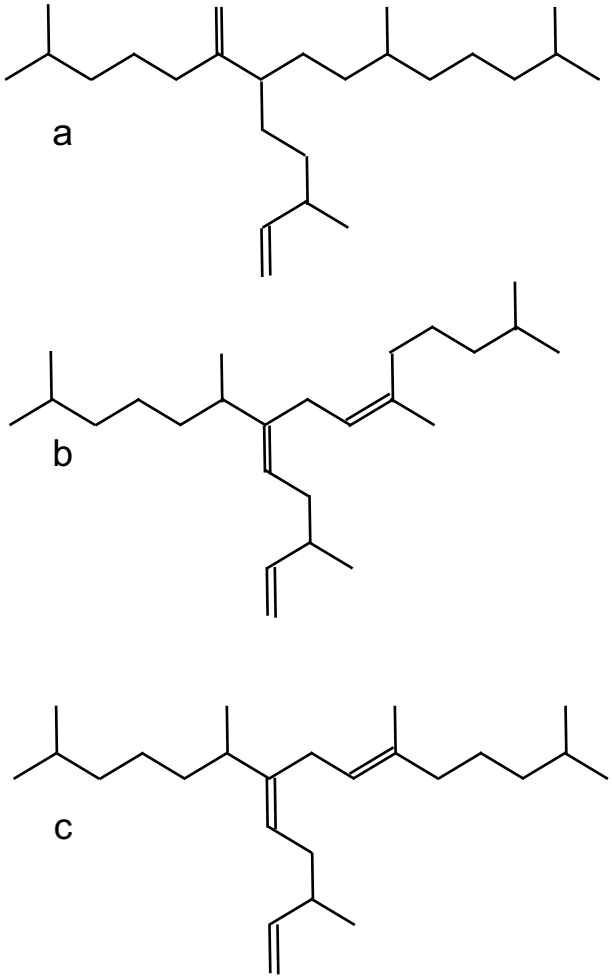

Figure 1: The molecular structures of a) $IPSO_{25}$, b) the HBI Z-triene, and c) the HBI E-triene.

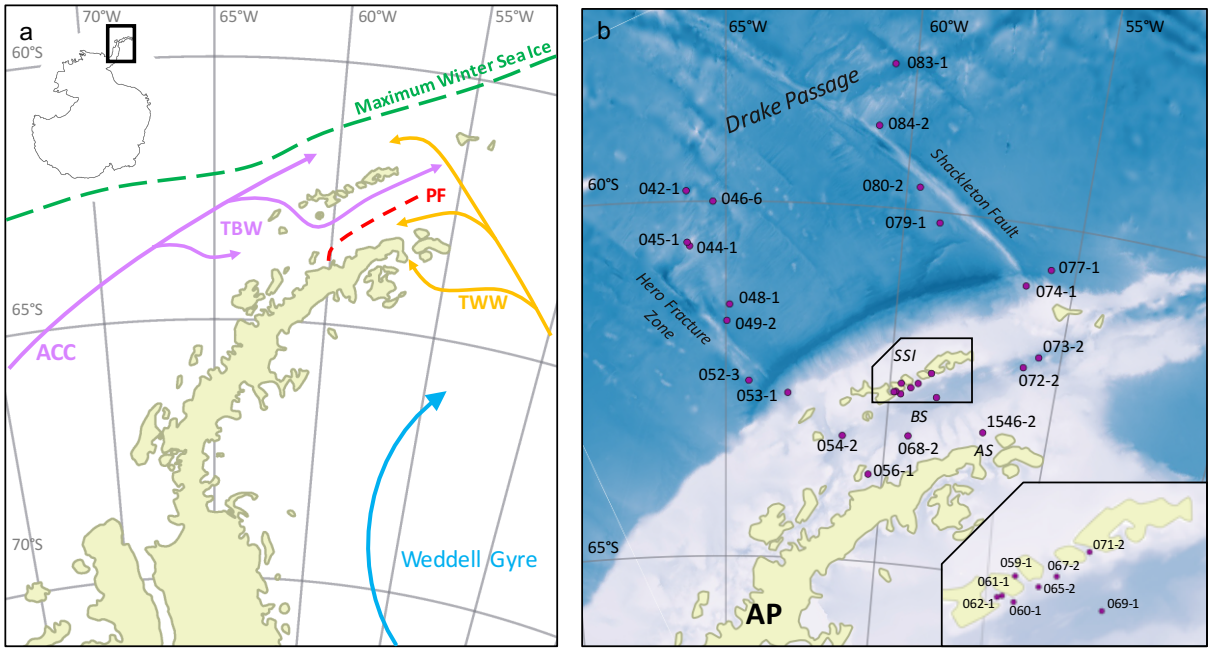

Figure 2: a) Oceanographic setting of the study area (modified after Hofmann et al., 1996; Sangrà et al., 2011) with ACC = Antarctic Circumpolar Current, TBW = Transitional Bellingshausen Water, TWW = Transitional Weddell Water, and PF = Peninsula Front, and the maximum winter sea ice extent (after Cárdenas et al., 2018). b) The bathymetric map of the study area with locations of all stations; AP = Antarctic Peninsula, AS = Antarctic Sound, BS = Bransfield Strait, and SSI = South Shetland Islands. A detailed station map at the South Shetland Islands is integrated. The overview maps were done with QGIS 3.0 from 2018 and the bathymetry was taken from GEBCO_14 from 2015.

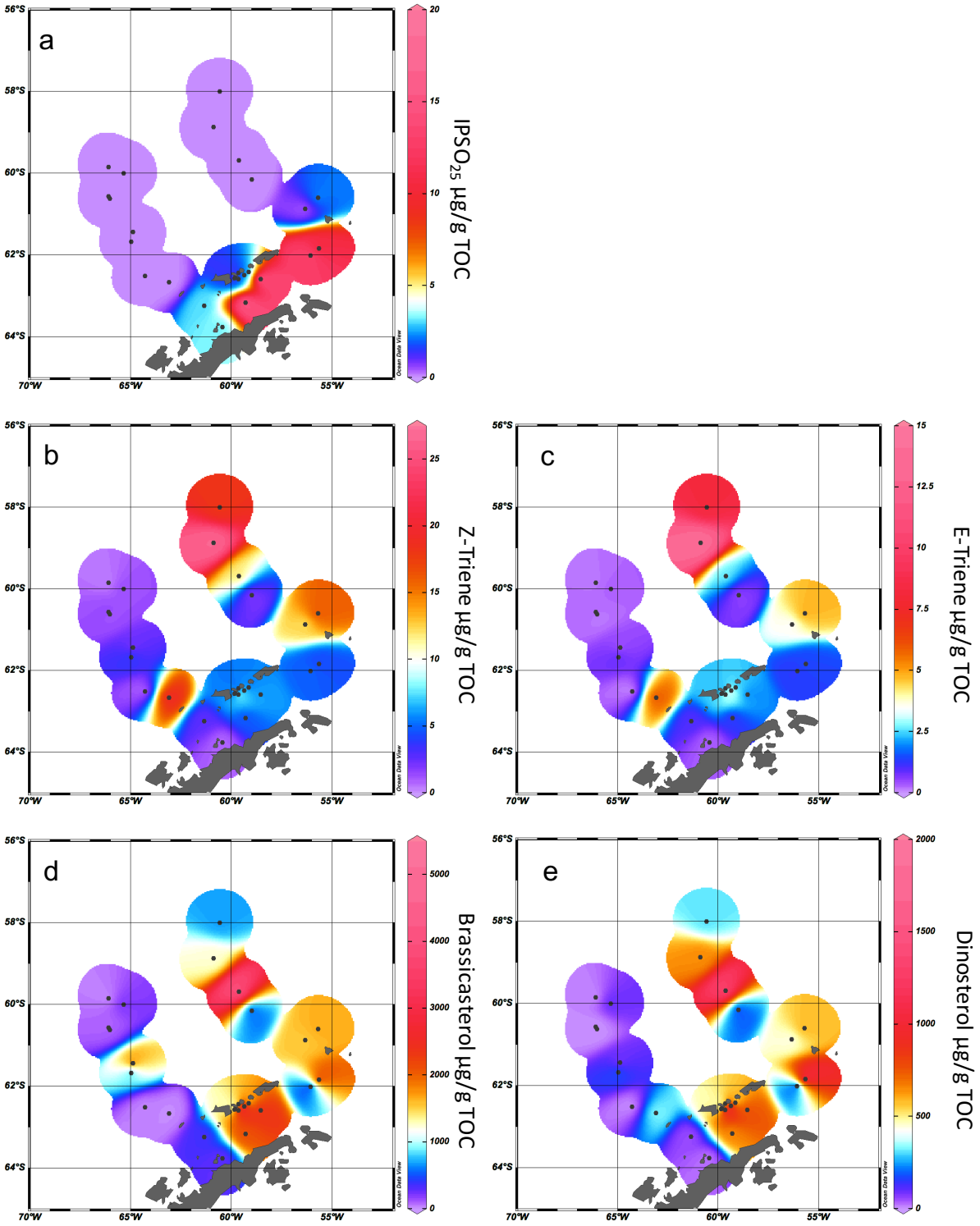

Figure 3: Distribution of a) $IPSO_{25}$, b) HBI Z-triene, c) HBI E-triene, d) brassicasterol, and e) dinosterol concentrations normalized to TOC. All distribution plots were made with Ocean Data View 4.7.10 (2017).

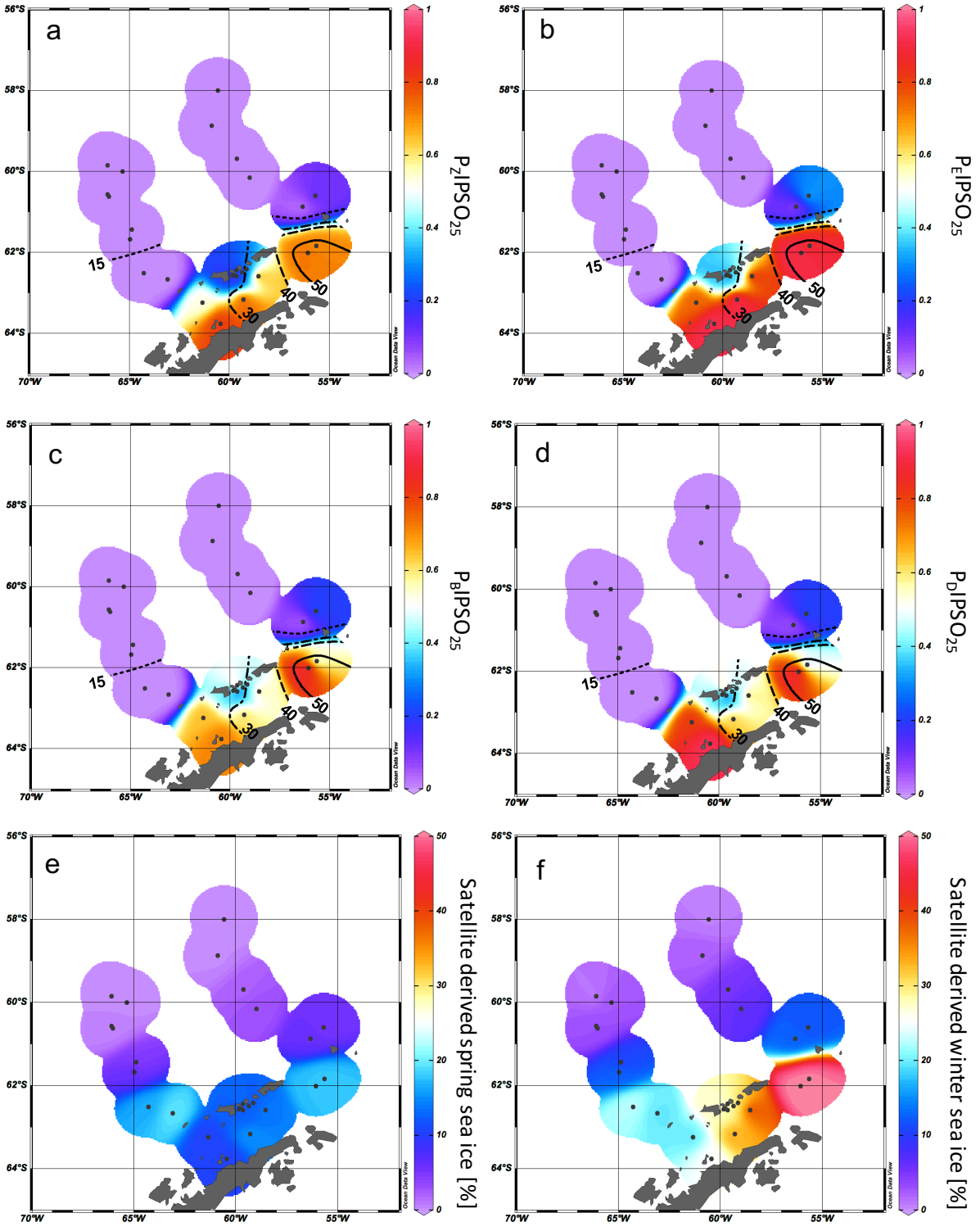

Figure 4: Distribution of a) P_ZIPSO_{25}, b) P_EIPSO_{25} , c) P_BIPSO_{25}, and d) P_DIPSO_{25} values in the study area. The extent of 15 %, 30 %, 40 % and 50 % satellite sea ice concentrations during winter is added as contour lines. Satellite derived mean sea ice concentrations at each sampling station are shown for e) spring and f) winter.

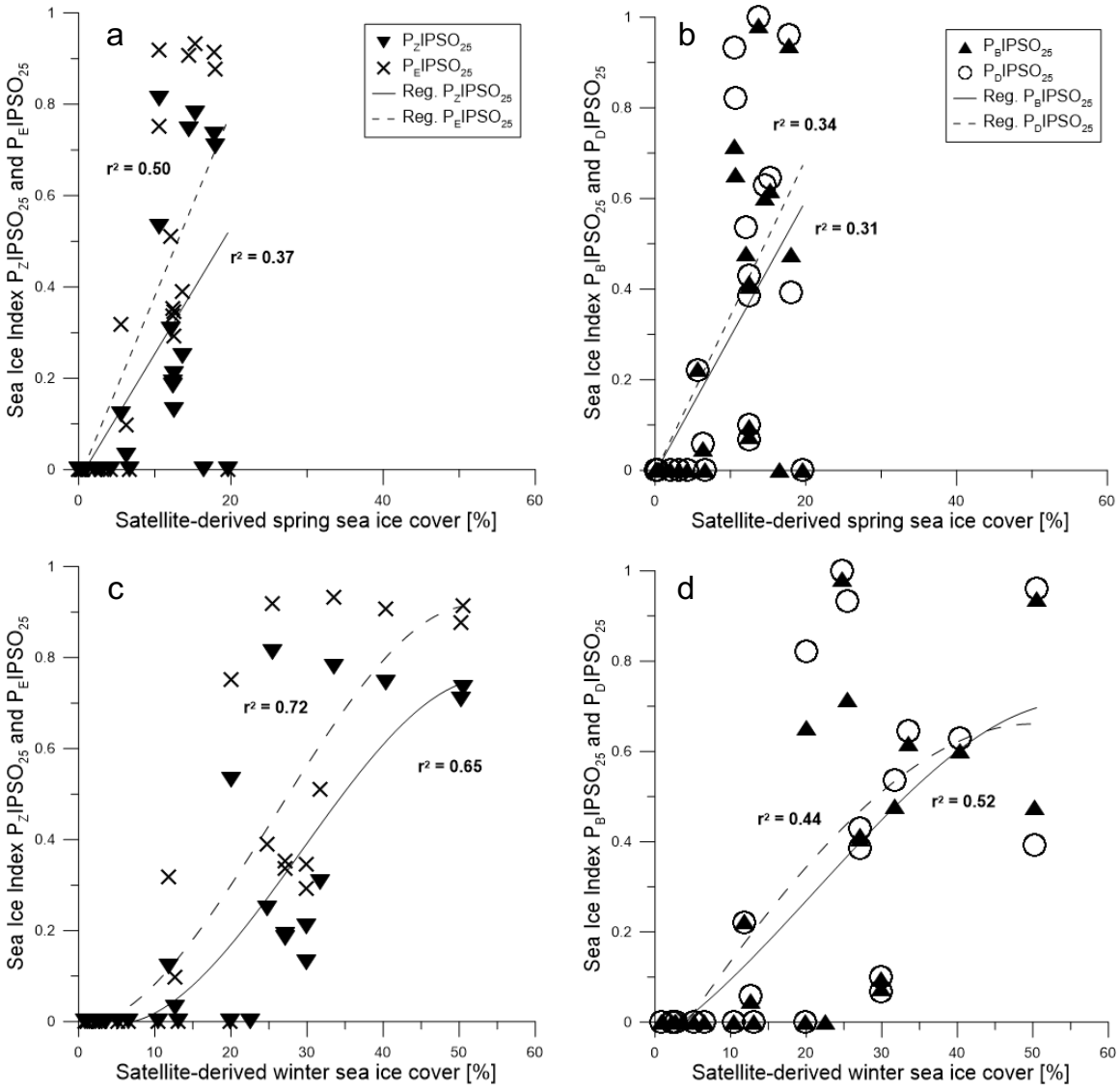

Figure 5: Scatter plots of satellite spring sea ice concentrations and a) P_ZIPSO_{25} (triangles, solid regression line) and P_EIPSO_{25} (crosses, dashed regression line) and b) P_BIPSO_{25} (triangles, solid regression line) and P_DIPSO_{25} (circles, dashed regression line). Scatter plots of satellite winter sea ice concentrations and c) P_ZIPSO_{25} (triangles, solid regression line) and P_EIPSO_{25} (crosses, dashed regression line) and d) P_BIPSO_{25} (black triangles, solid regression line) and P_DIPSO_{25} (circles, dashed regression line). All scatter plots were done with Grapher™ 13.

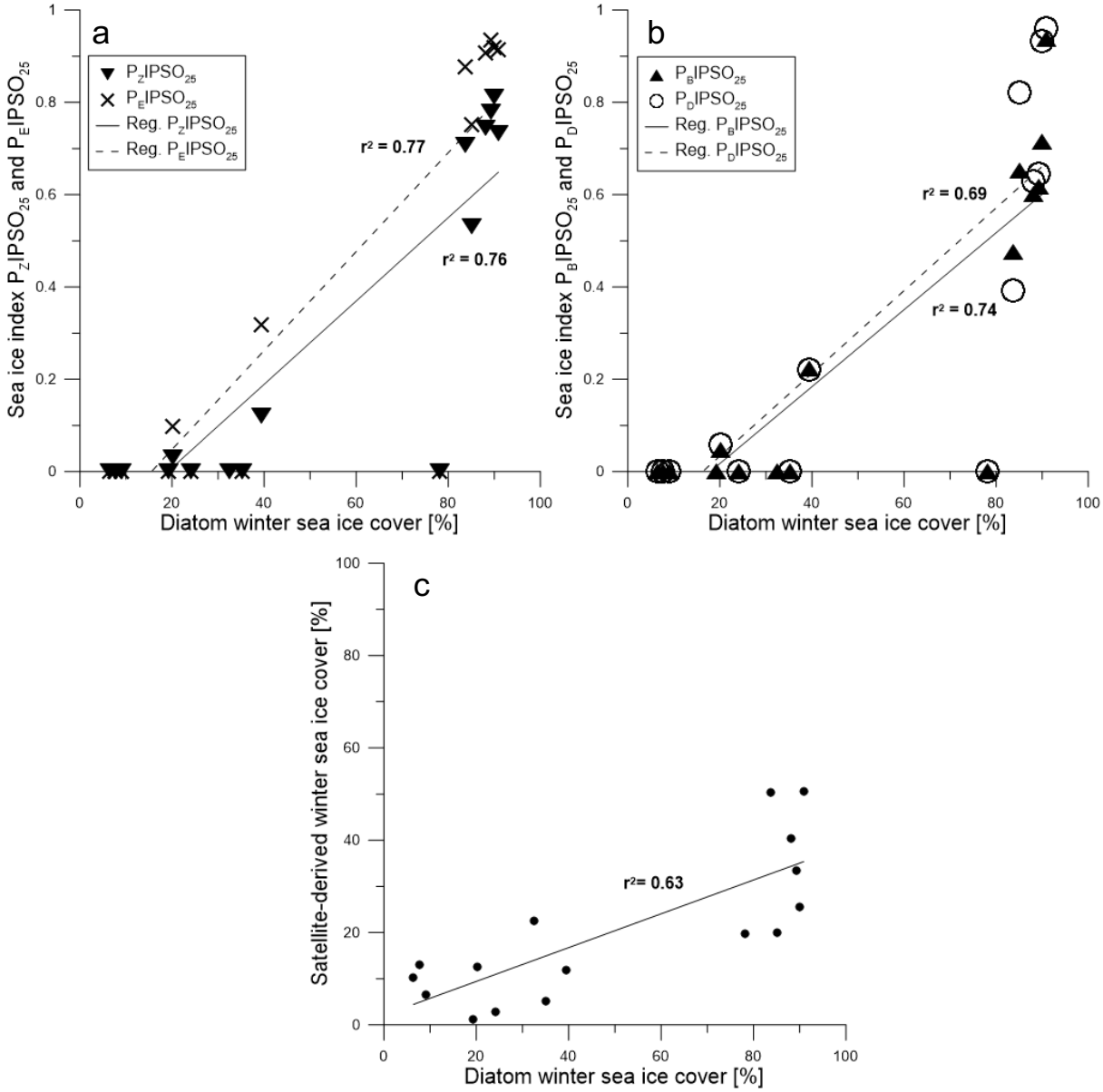

Figure 6: Scatter plots of a) P_ZIPSO_{25} (triangles, solid regression line) and P_EIPSO_{25} (crosses, dashed regression line) and b) P_BIPSO_{25} (triangles, solid regression line) and P_DIPSO_{25} (circles, dashed regression line) against diatom derived winter sea ice concentrations. c) Scatter plot of diatom transfer function winter sea ice concentrations and satellite winter sea ice concentrations.

Tables

Table 1: Coordinates of sample stations with water depth, concentrations of $IPSO_{25}$, Z- and E-trienes, brassicasterol and dinosterol normalized to TOC, $\delta^{13}C$ values for $IPSO_{25}$, and values of sea ice indices $PIPSO_{25}$ based on the Z- and E-triene, brassicasterol and dinosterol. Concentrations below the detection limit are expressed as 0. The $PIPSO_{25}$ could not be calculated where $IPSO_{25}$ and the phytoplankton marker is absent (blank fields).

Station	Lon	Lat	Water Depth	$IPSO_{25}$/TOC	HBI Z-Triene /TOC	HBI E-Triene /TOC	Brassi-casterol/TOC	Dino-sterol/TOC	$\partial^{13}C$ of $IPSO_{25}$	P_ZIPSO_{25}	P_EIPSO_{25}	P_BIPSO_{25}	P_DIPSO_{25}
	[dE]	[dN]	[m]	[µg/g TOC]	[µg/g TOC]	[µg/g TOC]	[µg/g TOC]	[µg/g TOC]	[‰]				
PS97/042-1	-66.10	-59.85	4172	0	0.333	0.152	12.997	0		0.000	0.000	0.000	
PS97/044-1	-66.03	-60.62	1203	0	1.080	0	143.688	0		0.000		0.000	
PS97/045-1	-66.10	-60.57	2292	0	1.531	0.386	36.902	0		0.000	0.000	0.000	
PS97/046-6	-65.36	-60.00	2803	0	1.359	0.291	214.634	101.809		0.000	0.000	0.000	0.000
PS97/048-1	-64.89	-61.44	3455	0	2.085	0.375	1859.609	73.532		0.000	0.000	0.000	0.000
PS97/049-2	-64.97	-61.67	3752	0	3.924	0.851	719.155	178.446		0.000	0.000	0.000	0.000
PS97/052-3	-64.30	-62.51	2890	0	0.679	0	26.554	0		0.000		0.000	
PS97/053-1	-63.10	-62.67	2021	0	19.350	5.948	13.356	332.868		0.000	0.000	0.000	0.000
PS97/054-2	-61.35	-63.24	1283	3.033	2.675	1.000	337.686	48.579	-14.741	0.531	0.752	0.652	0.820
PS97/056-1	-60.45	-63.76	633	3.232	0.752	0.290	268.190	17.158	-10.3 ± 0.9	0.811	0.918	0.716	0.932
PS97/059-1	-59.66	-62.44	354	0.835	2.523	1.305	3.386	0.0002		0.249	0.390	0.981	0.999
PS97/060-1	-59.65	-62.59	462	1.934	12.937	4.693	5017.437	1983.750		0.130	0.292	0.074	0.066
PS97/061-1	-59.80	-62.56	467	1.018	4.341	1.870	302.356	119.512		0.190	0.352	0.413	0.383
PS97/062-1	-59.86	-62.57	477	0.907	4.044	1.787	276.372	88.272		0.183	0.337	0.407	0.428
PS97/065-2	-59.36	-62.49	480	2.416	9.184	4.549	4788.292	1587.309		0.208	0.347	0.095	0.100
PS97/067-2	-59.15	-62.42	793	1.785	4.038	1.710	406.567	113.728		0.307	0.511	0.478	0.533
PS97/068-2	-59.30	-63.17	794	16.206	4.558	1.152	2096.690	653.977	-14.1 ± 0.6	0.780	0.934	0.617	0.643
PS97/069-1	-58.55	-62.59	1642	17.814	6.115	1.824	2472.025	774.345	-12.6 ± 0.4	0.744	0.907	0.601	0.626
PS97/072-2	-56.07	-62.01	1992	13.689	4.997	1.277	192.625	40.686	-13.6 ± 0.3	0.733	0.915	0.937	0.961
PS97/073-2	-55.66	-61.84	2624	10.369	4.283	1.451	2388.458	1180.752		0.708	0.877	0.476	0.390
PS97/074-1	-56.35	-60.87	1831	0.371	12.075	3.409	1539.629	438.073		0.030	0.098	0.048	0.058
PS97/077-1	-55.71	-60.60	3587	2.267	16.356	4.874	1647.616	589.731		0.122	0.317	0.223	0.219
PS97/079-1	-59.00	-60.15	3539	0	1.893	0.510	479.917	154.400		0.000	0.000	0.000	0.000
PS97/080-2	-59.64	-59.68	3113	0	12.021	2.705	4019.003	1329.129		0.000	0.000	0.000	0.000
PS97/083-1	-60.57	-58.00	3756	0	18.256	8.280	686.502	308.610		0.000	0.000	0.000	0.000
PS97/084-2	-60.88	-58.87	3617	0	26.857	13.871	1245.652	648.474		0.000	0.000	0.000	0.000

11

Table 2: Seasonal sea ice concentrations from satellite observations for spring, summer, autumn and winter with standard deviations.

Station	Sea Ice Spring [%]	Sea Ice Spring StDev [%]	Sea Ice Summer [%]	Sea Ice Summer StDev [%]	Sea Ice Autumn [%]	Sea Ice Autumn StDev [%]	Sea Ice Winter [%]	Sea Ice Winter StDev [%]
PS97/042-1	0.04	0.19	0.00	0.00	0.01	0.05	1.14	5.00
PS97/044-1	0.92	3.25	0.02	0.23	0.00	0.00	3.67	9.38
PS97/045-1	0.52	2.08	0.01	0.08	0.00	0.04	2.65	7.81
PS97/046-6	0.29	1.35	0.00	0.00	0.00	0.00	2.84	8.55
PS97/048-1	4.22	8.52	0.00	0.00	0.00	0.00	10.36	18.17
PS97/049-2	6.65	11.85	0.00	0.00	0.00	0.04	13.02	19.91
PS97/052-3	16.48	21.62	0.40	2.95	0.04	0.31	22.59	24.94
PS97/053-1	19.59	23.59	0.29	2.45	0.04	0.35	19.86	24.13
PS97/054-2	10.62	15.18	0.44	0.79	0.76	2.62	20.06	20.72
PS97/056-1	10.55	16.21	4.73	3.25	2.77	4.44	25.47	23.02
PS97/059-1	13.67	16.13	4.23	2.25	5.03	5.48	24.77	20.33
PS97/060-1	12.53	16.84	1.87	2.15	5.43	9.24	29.93	22.05
PS97/061-1	12.43	16.18	1.86	2.07	4.15	7.30	27.14	21.31
PS97/062-1	12.43	16.18	1.86	2.07	4.15	7.30	27.14	21.31
PS97/065-2	12.53	16.84	1.87	2.15	5.43	9.24	29.93	22.05
PS97/067-2	12.08	17.22	0.82	1.88	5.60	10.10	31.74	22.69
PS97/068-2	15.30	19.35	4.89	3.40	6.44	10.45	33.49	23.13
PS97/069-1	14.51	19.85	0.40	2.34	7.83	13.78	40.41	24.27
PS97/072-2	17.74	22.74	1.46	5.38	16.69	20.35	50.49	25.09
PS97/073-2	17.99	23.28	1.81	6.14	16.43	19.85	50.29	26.01
PS97/074-1	6.30	13.65	0.02	0.12	0.55	2.29	12.65	19.30
PS97/077-1	5.60	12.20	0.04	0.13	0.77	2.99	11.83	17.81
PS97/079-1	3.10	8.91	0.03	0.27	0.01	0.12	6.50	15.49
PS97/080-2	2.08	7.52	0.01	0.08	0.00	0.04	5.14	14.17
PS97/083-1	0.03	0.23	0.00	0.00	0.00	0.04	0.87	4.27
PS97/084-2	0.40	2.21	0.00	0.00	0.00	0.04	2.23	9.59

Table 3: Details of the radiocarbon dates and calibrated ages.

Sample Name	AWI-No.	Material	$F^{14}C \pm$ error	Conventional ^{14}C age [a]	Calibrated age (cal BP) [a]
PS97/044-1	1657.1.1	N. pachyderma	0.5076	5447 ± 111	4830
PS97/059-2	1434.1.1	calcareous	0.8507	1299 ± 49	100
PS1546-2	1602.1.1	Moll.-Echinod	0.8456	1347 ± 64	142

Table 4: Estimations of winter sea ice (WSI) derived from diatom species and the distribution of main diatom species in each sample.

Station	Diatoms WSI (4an)	A.tabularis	E.antarctica	F.vanheurckii	F.kerguelensis	F.obliquecostata	F.sublinearis	F.curta	F.cylindrus	N.directa	O.weißflogii	P.lineola-turgid.-gr.	R.alata	R.hebetata fo. semispina	S.microtrias	T.lentiginosa	T.oliverana	Thalassiosira MT 3	P.pseudodenticulata	Stephanopyxis sp.
	[%]	[%]	[%]	[%]	[%]	[%]	[%]	[%]	[%]	[%]	[%]	[%]	[%]	[%]	[%]	[%]	[%]	[%]	[%]	[%]
PS97/042-1	19.2	0	0	0	0.8	0	0	0	0	0	0	0	0	0	0	0	0	0	0	0
PS97/046-6	24.2	0	0	0	0.8	0	0	0	0	0	0	0	0	0	0	0	0	0	0	0
PS97/048-1	6.4	0	0	0	0.8	0	0	0	0	0	0	0	0	0	0	0	0	0	0	0
PS97/049-2	7.7	0	0	0	0.7	0	0	0	0	0	0	0	0	0	0	0	0	0	0	0
PS97/052-3	32.4	1.4	4.3	0	60.3	0.2	0	0.9	0	0	0.5	0	0	0	0	16.2	0.5	0	0	0
PS97/053-1	78.1	0.4	1.2	0	48.5	0.1	0.1	7.4	0.3	0	0.4	0	0.3	0	0.1	6.5	0	0	0	0
PS97/054-2	85.2	0	0.4	0	6.2	0	0	6.9	0.4	0.2	2.7	0.2	0.2	0.2	0.4	0.9	0	0.2	0	0.4
PS97/056-1	89.9	0	0	0	0.5	0.3	0	1.9	0.5	0.3	0.5	0	0	0	0.5	0.5	0	0.0	0.5	0.3
PS97/068-2	89.2	0	0	0	0.7	0.3	0.6	4.9	2.4	0.1	0.5	0.1	0	0	0.4	0.4	0	0.4	0.2	0
PS97/069-1	88.2	0	0.2	0.4	2.1	0.2	0.4	4.3	1.3	0	0.6	0.2	0	0	0.2	0.4	0	0.2	0	0
PS97/072-2	90.9	0	0.2	1.1	1.7	0.6	0.9	8.1	0	0	5.7	0.2	0.2	0	0	1.7	0	0.9	0.9	0
PS97/073-2	83.7	0	0.2	0.2	1.8	0	0.4	7.4	1.0	0	1.0	0	1.6	0.8	0	0.4	0	2.1	0.6	0
PS97/074-1	20.1	0.4	0.6	0	63.1	0	0	2.3	0	0	0.2	0	0.0	0.2	0	7.4	0.4	0	0.2	0
PS97/077-1	39.4	0.6	3.3	0	49.1	0.8	0	3.1	0.2	0	0.2	0	0.0	1.3	0	10.0	0.2	0	0	0
PS97/079-1	9.1	0	0	0	0.7	0	0	0	0	0	0	0	0	0	0	0	0	0	0	0
PS97/080-2	35.1	0	0	0	0.7	0	0	0	0	0	0	0	0	0	0	0	0	0	0	0